# Rotational and Vibrational State Distributions of HNC(0 $v_2^1$ 0) from the Hot H Atom Reaction: H + $(CN)_2$ → HNC + CN†

**R. Glen Macdonald***

*Argonne National Laboratory, Chemistry Division, 9700 South Cass Ave., Argonne, Illinois 60439*

*Received: March 20, 2000; In Final Form: June 1, 2000*

The reaction dynamics of the five-atom system, H + $(CN)_2$, was investigated by probing the minor product channel producing the transient HNC molecule. The complete initial energy disposition, translation, rotation, and vibration was determined for the HNC(0 $v_2^1$ 0), $v_2^1 = 0^0, 1^1$, product. The reaction was studied under bulk conditions and was initiated by energetic H atoms with a mean translational energy of 92 kJ $mol^{-1}$. The HNC molecule was monitored by time- and frequency-resolved absorption spectroscopy with sub-Doppler resolution. The initial rotational state distribution of each HNC(0 $v_2^1$ 0) vibrational level was measured and found to be well-described by a Boltzmann distribution. Only two vibrational levels were detected so that the initial HNC product vibrational level distribution was determined as well. The absolute reaction cross section for the title reaction was measured to be $2 \times 10^{-18}$ $cm^2$ for H atoms with a nominal translational energy of 113 kJ $mol.^{-1}$

## I. Introduction

The details of the energy disposal in three atom systems have greatly added to our understanding of reaction dynamics. Indeed, the interaction between theoretical predictions and experimental observations have resulted in the emergence of some very useful global concepts.[1,2] The current status of atom + diatom systems is such that it now almost possible to completely determine the reaction dynamics between atoms and molecules composed of first row elements using first principles, i.e., using the calculation of an ab initio potential energy surface (PES) and a complete quantum mechanical treatment of the scattering dynamics.[3]

Naturally, there has been a significant trend over the past few years to extend the detailed study of reaction dynamics into systems involving more than three atoms. For those studies interested in probing reaction dynamics by investigating the energy disposal into the reaction products, with a few exceptions, the studies have concentrated on probing the diatomic product in a state-specific manner. Efforts to probe the internal state distribution of the polyatomic reaction product are hampered by the large number of internal states, rotational and vibrational, that are accessible to a polyatomic molecule and a general difficulty in applying state-specific laser techniques to polyatomic species. To circumvent these difficulties, most investigators probing the energy disposition into a polyatomic reaction product have concentrated on determining the vibrational level distribution only and not the determination of the initial rotational state distribution. All polyatomic molecules have active infrared absorptions so either infrared absorption or chemiluminescence have been the experimental method of choice to detect the vibrational level distribution of the polyatomic product.[4,5,6,7,8,9,10,] The CN + $O_2$ → NCO + O is the only four-atom system in which the vibrational[11,12] and rovibrational state distributions[13] in the polyatomic product have been probed by laser-induced fluorescence.

Much of our understanding of the energy disposition into the polyatomic product comes from theoretical studies of four atom systems, using both quasiclassical trajectory calculations[14] or approximate quantum scattering methods.[15,16] The problem of dealing with nine internal degrees of freedom from first principles is still an intractable computational problem for exact quantum scattering calculations, but progress is rapidly being made.[3] A recent review summarizes the details of the comparison between theory and experiment for four atom systems.[17] An example of the complexity of a global PES involving four atoms is provided by the HClCN system, for which Harding calculated 9 transition states and 14 minima.[18]

An excellent example of the interplay between theory and experiment to elucidate the reaction dynamics in a polyatomic system is provided by the OH + HBr → $H_2O$ + Br reaction and its istopomers.[10] The vibrational energy distributions of the various possible $H_2O$ isotopomers were determined by infrared chemiluminescence measurements. Quasiclassical trajectory calculations[19] were carried out on a model PES and were used to elucidate the mechanism for vibrational energy disposition into the $H_2O$ product. The calculations suggested several methods for producing the large bending excitation observed experimentally, and further illustrated that kinematic effects for a $\boldsymbol{H} + \boldsymbol{L} - \boldsymbol{H}$ (where $\boldsymbol{H}$ and $\boldsymbol{L}$ are heavy and light masses, respectively) mass combination expected for triatomic systems were valid in the tetratomic case as well.

In the present work, the reaction dynamics of the pentatomic reaction system H + $(CN)_2$ → HNC(0 $v_2^1$ 0) + CN were explored by determining the rotational state distribution of the HNC product in its ground and first excited bending vibrational level. The vibrational population distributed between these two levels was also determined. No other rovibrational transitions were detected, so these measurements likely determine the vibrational level distribution in the HNC product. As a further probe into the reaction dynamics of this system, the center of mass (COM) translational energy disposition was also measured.

The reaction was initiated by photolyzing $CH_3SH$ at 248 nm creating energetic H atoms that reacted with $(CN)_2$ at low

† Part of the special issue "C. Bradley Moore Festschrift".

* To whom correspondence should be addressed. E-mail: macdonald@anlchm.chm.anl.gov.

10.1021/jp0010583 CCC: $19.00 
Published on Web 07/11/2000

pressures under bulk conditions. The HNC rovibrational population was probed by time- and frequency-resolved infrared absorption spectroscopy with sub-Doppler frequency resolution. The experiments reported here are closely related to other studies of H + XCN → HX + CN, where X = Br, Cl, or CN, from this laboratory.[20] In these experiments, the COM translation energy release and rotation state distribution of the CN(0, J) product were determined.

## II. Experimental Section

The basic experimental apparatus has been described in previous work,[21] but for completeness, a brief description is given here. The reaction chamber consisted of a vacuum-tight stainless steel chamber containing a Teflon box of interior dimensions of 100 × 100 × 5 cm. The chamber was evacuated by a liquid nitrogen trapped mechanical pump to a pressure of a few mTorr with a leak rate of less than 0.5 mTorr per minute. Equal flow rates of $(CN)_2$ and $CH_3SH$ (both gases supplied by Matheson) were delivered from separate vacuum systems and continuously flowed through the apparatus. The partial pressures of the reagents were calculated from their known flow rates and total chamber pressure, which was between 0.090 and 0.100 Torr.

The photolysis laser was a Lambda Physik Compex 205 excimer laser operating at 248 nm. A portion of the excimer laser radiation transmitted through the apparatus was monitored by a Molectron J-50 power meter. This measurement was used to correct the data for variations in the photolysis laser intensity caused by pulse-to-pulse fluctuations and a gradual decrease in intensity due to a build-up of a UV absorbing deposit on the optical surfaces exposed to the UV radiation.[20]

Individual rovibrational levels of HNC were detected by time- and frequency-resolved infrared absorption spectroscopy. The continuous wave infrared laser source was a Burleigh Model 20 single mode color center laser. The HNC rovibrational line positions were taken from Burkholder et al.[22] and data from this laboratory.[23] The absolute frequency of the infrared laser was determined by a Burleigh Model WA-20IR wavemeter to an accuracy of about 200 MHz, and a Model CF-500 high finesse Etalon with a free spectral range of 150 MHz.

As described previously,[21] the infrared probe laser was multipassed through the photolysis zone using White cell optics. Both the probe and photolysis laser beams were aligned collinearly using a UV−IR dichroic mirror mounted on the optical axis of the White cell at Brewster's angle, with respect to the IR laser beam.

The transmitted intensity of the infrared probe laser was monitored by a liquid nitrogen cooled InSb detector. The frequency response of the detector and associated electronics was better than 7 MHz. The largest source of noise in the experiment was caused by low-frequency fluctuations of the probe laser intensity. To suppress this noise source, a portion of the probe laser intensity was monitored by a second liquid nitrogen cooled InSb detector. The output of this detector was used as the reference for a Cambridge Research optical modulator that controlled the optical power from the Krypton ion laser used to pump the color center laser. This closed-loop feedback system resulted in reduced fluctuations of the probe laser intensity. To further suppress low-frequency noise, the transient absorption signal was passed through an electronic high pass filter.

Four Stanford model SR-250 boxcar integrators were used to record the transient absorption signal. One boxcar was used to record the initial laser intensity, $I_o$, measured at 100 $\mu$s before the photolysis laser pulse, and the other three recorded absorptions at observation times of 0.3, 0.6, and 20 $\mu$s following the initiation of the reaction. The gates of the boxcars monitoring the transient absorptions were 0.1 $\mu$s wide, centered on the nominal observation time. After 20 $\mu$s, the HNC was in thermal equilibrium with the reagent gases, and the transient absorption signals slowly decreased due to diffusion and flow. The experiment was controlled by a laboratory PC that provided the necessary timing pulses to initiate the experiment and control voltages to scan the frequency of the color center laser.

The HNC molecule is a moderately light, linear hydride so that the spacing between rovibrational levels is several wavenumbers compared to a 293 K Doppler width of only 0.008 wavenumbers. This large spacing between absorption features precluded long frequency scans and only individual absorption features were scanned. The laser frequency was incremented in about 10 to 20 MHz steps. At each step, the excimer laser was fired for 20 to 50 pulses, and the signal from each boxcar recorded and averaged. The color center laser cavity was adjusted from line-to-line so that the calibration factor relating the scan voltage to the absolute frequency of the laser also varied. The probe laser frequency scale was calibrated by simultaneously monitoring the output from the high resolution CF-500 Etalon. A scan consisted of about 8 to 10 Etalon fringes. As noted, the probe laser was scanned in discrete frequency increments, and the occasional Etalon fringe would be missed. However, this situation was readily apparent over a complete scan. The calibration factor relating control voltage to laser frequency was determined from a linear least-squares fit to the accumulated Etalon frequency measurement and control voltage with an uncertainty of about ± 1%.

For each vibrational state, a single transition near the peak in the rotational state distribution was used to normalize the data. After 3 to 5 rotational states were scanned, the normalization level was rescanned. This procedure allowed scans recorded on separate days to be related to each other and corrected for possible drifts in experimental parameters.

## III. Results

**A. Analysis.** The reaction sequence initiated by the translationally energetic H atoms is given by:

$$CH_3SH \xrightarrow{248nm} CH_3S + H, \quad (1)$$

$$H + (CN)_2 \rightarrow HCN + CN, \quad (2a)$$

$$\rightarrow HNC + CN, \quad (2b)$$

$$CN + CH_3SH \rightarrow HCN + CH_3S/CH_2SH, \quad (3a)$$

$$\rightarrow HNC + CH_3S/CH_2SH \quad (3b)$$

All species were lost by diffusion, but over the observation time of several ten's of $\mu$s, the diffusion was not important. The branching fractions into the HCN and HNC channels for reactions 2 and 3 are currently under investigation.[24] Preliminary data indicate that the thermal rate constant for reaction 3 is nearly gas kinetic, and that the branching fraction, $k_{ib}/(k_{ia} + k_{ib}) \sim 0.1$, for both reactions 2 and 3, where $k_i$ is the thermal rate constant for reaction i.

The H atom translational distribution from reaction 1 was calculated from the measured distribution[25] from the 243.1 nm photolysis of $CH_3SH$ and the known photochemistry[26] and photodynamics[27] occurring at 248 nm. The H atoms produced in reaction 1 have a Gaussian distribution with a mean

translational energy, $\bar{E}_{\text{H}}$, of 92 kJ mol$^{-1}$ and a fwhm of 38 kJ mol$^{-1}$. The H atom distribution is initially orientated with a $\beta$ parameter near $-1$; however, Park et al.[28] have measured the relaxation of a similarly orientated H atom distribution produced from the photolysis of $H_2S$ at 193 nm. As previously argued,[20] elastic reorientation collisions have a much larger cross section than inelastic collisions, and at the relatively long delay time of 0.3 $\mu$s, the H atom distribution should be isotropic.

Even though the photolysis laser was unpolarized, the collinear propagation of the probe and photolysis lasers eliminated the possibility of experimentally detecting any anisotropy in the HNC speed distributions. Furthermore, even if the COM differential cross section for the HNC product were highly directional, the nearly isotropic and broad H atom speed distribution, multiple correlated CN(0,J) product states, and initial thermal $(CN)_2$ speed distribution, would all contribute to blur the observation of any anisotropy. Hence, it was assumed that the HNC product speed distribution was isotropic, and the area of an absorption feature determined the population in the absorbing level.

For an absorption between two states j ← i, the absorption coefficient at frequency $\nu$, $\sigma(\nu)$, is related to the integrated line strength, $S_{\text{ji}}$, for the transition by the normalized line shape function, g($\nu$), as $\sigma(\nu) = S_{\text{ji}}\, g(\nu)$. The absorbance at $\nu$, $A(\nu)$, is given by the Beer−Lambert law as[29]

$$\text{A}(\nu) = \ln\left(\frac{I_o(\nu)}{I(\nu)}\right) = 1\ \sigma(\nu)\left([\text{N}_i] - \frac{g_i}{g_j}[\text{N}_j]\right) \qquad (4)$$

where $I_o(\nu)$ and $I(\nu)$ are the incident and transmitted light intensities at $\nu$, l is the path length, $g_i$ is the degeneracy of level i, and [ $N_i$] is the total concentration of absorbers in level i. Provided that the population in the upper level, j, is zero, integration of eq 4 over frequency relates the concentration, [$N_i$], to the area under an absorption line and the integrated line strength, $S_{\text{ji}}$, by

$$[\text{N}_i] = \frac{\int_{-\infty}^{\infty} A(\nu)}{1 \int_{-\infty}^{\infty} \sigma(\nu)\text{d}\nu} \qquad (5)$$

where the integral in the denominator is given by $S_{\text{ji}}$.

Only two HNC vibrational levels were detected in the present experiments, the ground-state HNC(00°0) and the first excited bending state HNC(01$^1$0). Both levels were probed using the fundamental H−NC $\Delta\nu_1 = 1$ vibrational transition as the active chromophore. The transition moment for the HNC (10$^0$0) ← (00$^0$0) fundamental transition has recently been measured[30] so that the $S_{\text{ji}}$ for the rovibrational transitions probed in the present experiment can be calculated from[31]

$$S_{\text{ji}} = \frac{8\pi^3}{3hc}\bar{\nu}_{\text{ji}}\, |\langle \text{j}|\mu|\text{i}\rangle|^2\, \frac{A_{\text{ji}}}{2J+1}\, \text{HW} \qquad (6)$$

where $c$ and $h$ have their usual meanings, $\bar{\nu}_{\text{ji}}$, is the wavenumber of the transition, $|\langle \text{j} \mid \mu \mid \text{i}\rangle|$ is the vibrational transition moment, $A_{\text{ji}}$ is the appropriate Hönl−London factor, and HW is the Herman−Wallis factor, accounting for the interaction between rotation and vibration. The HW factor can be expressed as $(1 + A_1 m + A_2 m^2)^2$ where $m$ is $J + 1$ for an R branch and $-J$ for a P branch. For the HNC(10$^0$0) ← (00$^0$0) transition, the HW have been determined;[32,23] however, they have not been measured for the HNC(11$^1$0) ← (01$^1$0) transition. The optical path length was defined by the distance between the UV−IR dichroic mirror and the UV beam absorber and the number of passes the probe laser made through the photolysis zone; hence, the absorption measurements provided an absolute determination of the HNC concentration produced in reaction 2b.

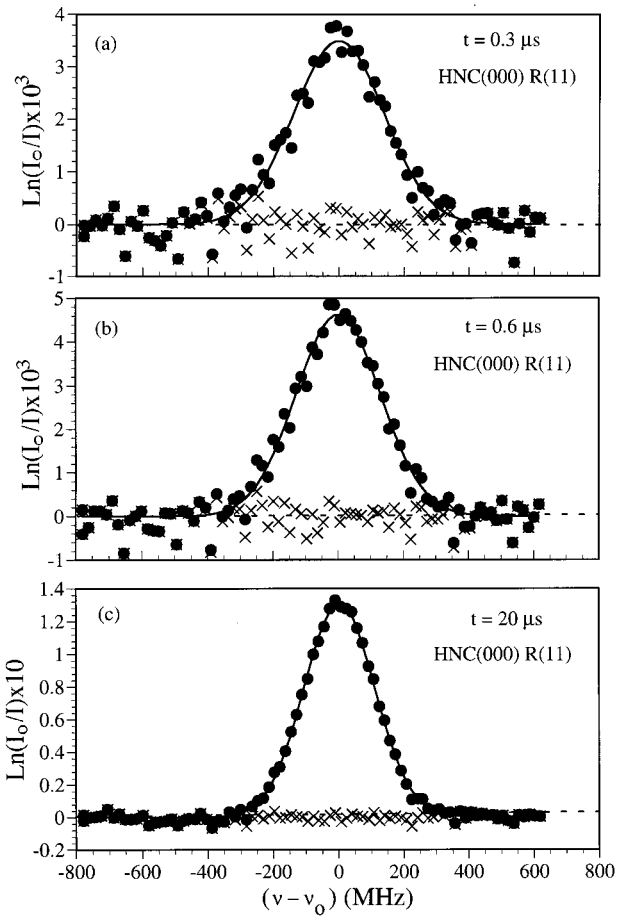


**Figure 1.** Absorption line profiles for $R(11)$ of the HNC(10$^0$0) ← HNC(00$^0$0) transition obtained at various observation times following the initiation of reaction 2b. The solid lines are Gaussian frequency profiles fit to the data, and the residues are indicated by the crosses. At a delay time of 20 $\mu$s, Panel (c), the HNC product had equilibrated to the temperature of the reaction chamber, 293 K. The conditions of the experiment were $P_{\text{CH3SH}} = 0.050$ and $P_{(\text{CN})2} = 0.050$ Torr for a KrF laser energy of 300 mJ/pulse. At 293 K, the Doppler width for the $R(11)$ transition is 262 MHz.

**B. Rotational State Distributions of HNC(00$^0$0) and HNC(01$^1$0).** Typical absorbance profiles for the three observation times are shown in Figure 1 for the HNC(10$^0$0) ← (00$^0$0) R(11) transition and for the HNC(11$^1$0) ← (01$^1$0) $R_f(11)$ transition in Figure 2. The solid line in each figure is a Gaussian frequency profile fit to the data, i.e., $A(\nu) = A_{\text{pk}}\exp(-((\nu-\nu_o)/a)^2)$. The three parameters describing the Gaussian profile were determined by a nonlinear least squares procedure based on Mardquart's method,[33] and the area under each absorbance feature was determined from the nonlinear least squares parameters as $\int_{-\infty}^{\infty} A(\nu)\text{d}\nu = A_{\text{pk}} a\sqrt{\pi}$. The crosses in Figures 1 and 2 indicate the difference between the experimental absorbance and the calculated profile. Note that the distribution of the residuals is uniform across the profile indicating that the Gaussian functional form adequately described the data. As will be discussed in Section D, the fwhm of the absorbance profiles for the first two boxcar delays are broader than the Doppler width describing a thermal (293 K) distribution so that the HNC products in the (00$^0$0) and (01$^1$0) vibrational states are initially produced with excess translational energy.

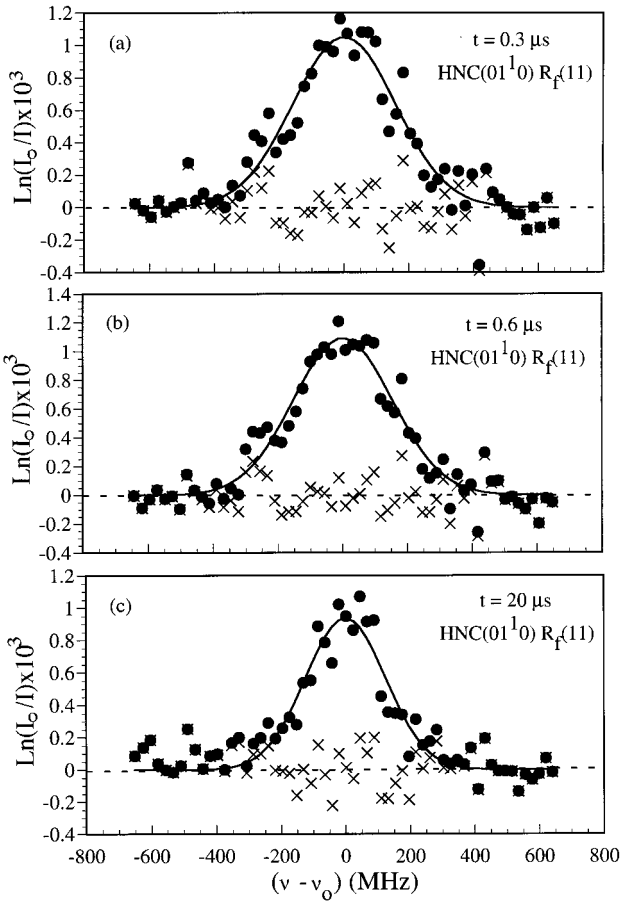


**Figure 2.** Same as Figure 1 except the $R_f(11)$ absorption line for the HNC($11^10$) ← HNC($01^10$) transition.

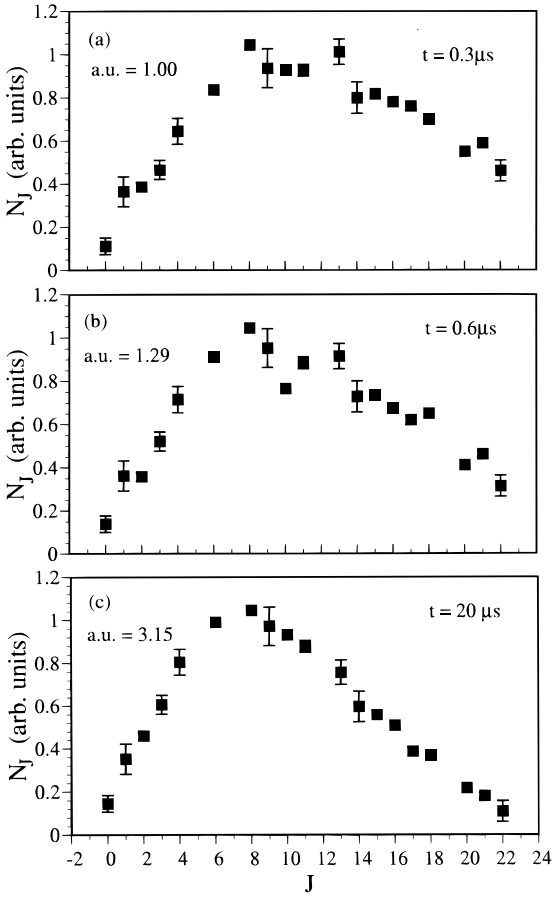


**Figure 3.** The rotational state distributions for HNC($00^00$) produced in reaction 2b measured at three different times following the initiation of the reaction. The initial rotational state distribution was that given at the shortest observation time panel (a). The distributions were measured relative to HNC($00^00$) $R(9)$ at $t = 0.3$ $\mu$s assigned a value of 1.

As noted earlier, pulse-to-pulse variations in the excimer laser power were monitored by recording a portion of the photolysis laser that was transmitted through the apparatus, $P_t$. As well, the gradual attenuation of the photolysis laser power by a deposit formed on the optical surfaces exposed to the UV laser radiation was accounted for by normalizing the absorbance data according to an experimentally determined power law, $A(\nu) \propto P_t^{0.6}$, as described previously.[20] The rotational state distributions in the HNC (0 $v_2^1$ 0) vibrational levels were determined by scanning over the R-branch of the HNC(1 $v_2^1$ 0) ← (0 $v_2^1$ 0) transitions. Only a few rotational levels were obscured by atmospheric absorptions. The use of P-branch transitions resulted in poorer signal-to-noise because the sensitivity of the apparatus decreased at longer wavelengths due to an increase in infrared absorption by the UV−IR dichroic mirror. One or two transitions for each vibrational level, $R(9)$ for HNC(000) and $R_{e/f}$ (9) or $R_{e/f}$ (10) for ($01^10$), were chosen to normalize the data collected over different time periods for each vibrational level. Also, some of these measurements, which were taken under identical experimental conditions, were used to determine the vibrational state distribution and will be discussed further in the next section.

The rotational state distributions for the HNC($00^00$) ground state measured at the three observation times of 0.3, 0.6, and 20 $\mu$sec are shown in Figure 3. The rotational state distributions shown in Figure 3 are the average of several distributions obtained under a variety of different experimental configurations such as photolysis laser power and optical path length. The different distributions were normalized to the population calculated for the [HNC($00^00$; $J = 9$)] state at each observation time using the measured rotational temperature for two distributions obtained under similar experimental conditions. The scale factor in each panel in Figure 3 relates the [HNC($00^00$; $J = 9$)] at the different times to each other with this average population at 0.3 $\mu$s given a value of 1. The error bars in Figure 3 indicate an uncertainty of one standard deviation ($\pm 1\sigma$) in the average of at least 4 independent measurements. For some rotational states, the uncertainty is smaller than the symbol size plotted in the figure.

The rotational state distributions shown in Figure 3 are plotted as Boltzmann plots in Figure 4. If the distribution can be described by a rotational temperature, $T_{rot}$, the Boltzmann plot is linear with slope equal to $-1/kT_{rot}$ and the intercept equal to $\ln([N(\nu)]_{tot}/Q_{rot})$, where the brackets [ ] indicate concentration, $[N(\nu)]_{tot}$ is the total concentration in the probed vibrational level $\nu$, i.e., $[N(\nu)]_{tot} = \sum_J [N(\nu; J)]$, and $Q_{rot}$ is the rotational partition function. As is evident from Figure 4, the rotational distributions were well-described by a temperature. The results of a linear least-squares analysis to determine $T_{rot}$ and $[N(\nu)]_{tot}$ are summarized in Table 1.

The $T_{rot}$ measured at an observation time of 20 $\mu$s was in good agreement with 293 K temperature of the reaction chamber. For an HNC molecule at a total pressure of 0.090 Torr, a time of 0.3 $\mu$s corresponds to about one-quarter of the hard sphere collision rate. As is evident from Table 1, some rotational relaxation has occurred from a reaction time of 0.3 to 0.6 $\mu$s; however, the relaxation was not extensive, implying that the $T_{rot}$ determined at the initial observation time provided

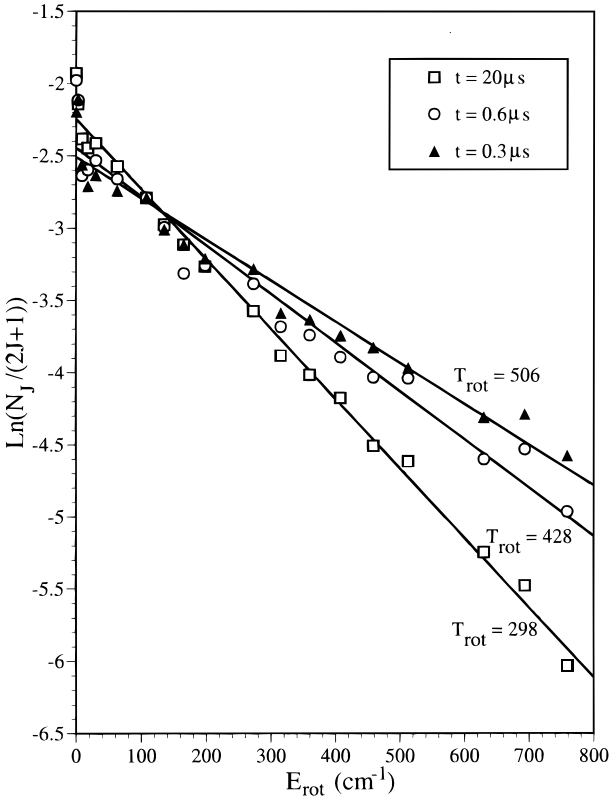


**Figure 4.** Boltzmann plot of the rotational state distributions shown in Figure 3. The linear least squares parameters are summarized in Table 1.

**TABLE 1: Summary of the Linear Least Squares Parameters Obtained from the Boltzmann Plots Shown in Figure 4 for the Rotational State Distribution for HNC(00°0) and in Figure 6 for the Rotational State Distribution for HNC(01$^1$0) Produced in the H + $(CN)_2$ Reaction[a]**

| HNC vibrational state | boxcar delay ($\mu$s) | $T_{rot}$ (K) | $[HNC(0\ v_2^1\ 0]_{tot}$ (arb units) |
|---|---|---|---|
| HNC(000) | 0.3 | 506 ± 26 | 18.9 ± 2.0[b] |
| | 0.6 | 428 ± 22 | 22.0 ± 2.6 |
| | 20.0 | 298 ± 6 | 45.4 ± 2.6 |
| HNC(01$^1$0) | 0.3 | 446 ± 77 | 34.4 ± 7.6[c] |
| | 0.6 | 393 ± 38 | 35.4 ± 4.6 |
| | 20.0 | 271 ± 20 | 28.2 ± 1.9[d] |

[a] The initial rotational state distribution was taken as that measured at the earliest observation time of 0.3 $\mu$s. The uncertainties for $T_{Rot}$ are $\pm 1\sigma$ from the least squares fit and for $[HNC(0v_2l\ 0]_{Tot}$. They include both the $\pm 1\sigma$ from the least squares fit and the calculated $Q_{Rot}$. [b] The [HNC(000; $J = 9$)] measured at a delay of 0.3 $\mu$s was assigned a value of 1 au [c] The [HNC(01$^1$0, $J = 9$,e or f] measured at a delay of 0.3 $\mu$s was assigned a value of 1 au. [d] The data were analyzed using the room temperature, 293 K.

a good description of the initial rotational state distribution in HNC(00$^0$0) produced in reaction 2b.

The rotational state distributions for the first bending vibration HNC(01$^1$0) are shown in Figure 5 for each observation time, and are presented as Boltzmann plots in Figure 6. The determinations of $T_{rot}$ and $[HNC(01^10)]_{tot}$ from a linear least-squares analysis are also summarized in Table 1. Similar to the presentation of the rotational state distribution for HNC(00$^0$0), the rotational state distributions for HNC(01$^1$0) were normalized to the [HNC(01$^1$0; $J = 9$] population calculated from the measured rotational temperature of two experiments recorded under identical conditions. The calculated [HNC(01$^1$0; $J = 9$] for the $T_{rot}$ obtained at an observation time of 0.3 $\mu$s was assigned a value of 1, and the arbitrary unit factors in Figure 5

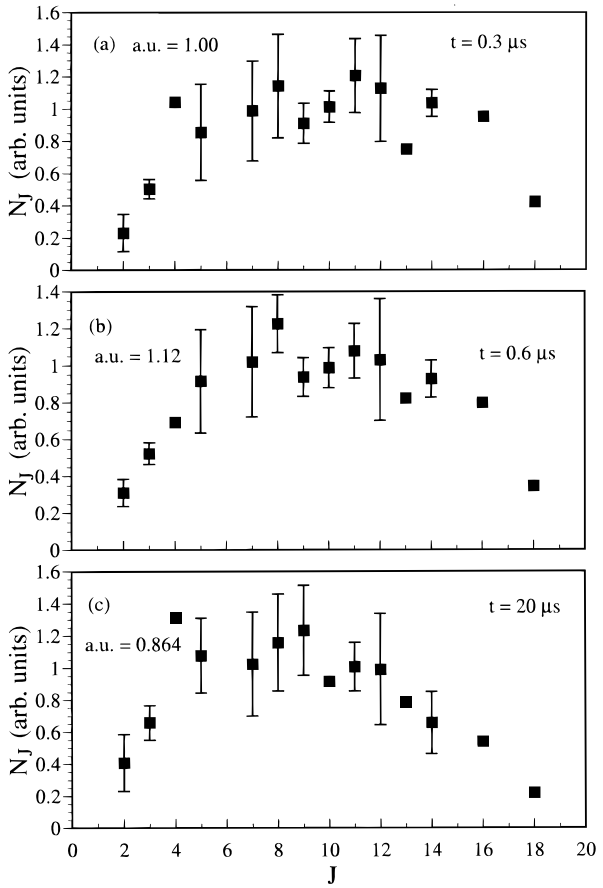


**Figure 5.** Similar to Figure 3 except the rotational state distributions for the HNC(01$^1$0) vibrational state at three observation times. The initial rotational state distribution is given in panel (a). The distributions were measured relative to HNC(01$^1$0) $R_{e/f}$ (9) at $t = 0.3$ $\mu$s assigned a value of 1.

relate to the other times. A comparison of the absorbance profiles in Figures 1 and 2 shows that the signal-to-noise was less for the HNC(01$^1$0) level and resulted in the increased scatter for the HNC(01$^1$0) rotational state distributions. Note that the populations in HNC(00$^0$0) and HNC(01$^1$0) were not directly related to each other by these measurements.

The doubly degenerate bending vibration of HNC has a fundamental frequency[22] of $\nu_2 = 464.2$ cm,$^{-1}$ and at 293 K, 16.5% of the HNC population is in the $\nu_2 = 1$. This is reflected in the measurement of the [HNC(01$^1$0)] at 20 $\mu$s, as will be discussed further in Section III C.

The dependence of $T_{rot}$ on the reaction times for the HNC(01$^1$0) vibrational level was similar to that found for HNC(00$^0$0), (see Table 1). The $T_{rot}$ measured at an observation time of 0.3 $\mu$s. was only slightly higher than that measured at 0.6 $\mu$s, and the increase in $[HNC(01^10)]_{tot}$ was small. Again, this indicates that the $T_{rot}$ measured at a reaction time of 0.3 $\mu$s. was a good measure of the initial rotational state distribution of HNC(01$^1$0) produced in reaction 2b. The fact that both vibrational levels increased by nearly the same fraction is strong evidence that both vibrational levels are produced in the same reaction.

**C. Vibrational Level Distribution for HNC.** The enthalpies, $\Delta H°$, for reaction 2a and 2b are summarized in Table 2. A large source of uncertainty comes from the $\Delta_f H_o$ for the CN radical. From the work of North and Hall[34] on the photodissociation dynamics of $(CN)_2$, a value of $\Delta_f H_o$ equal to 431.9 ± 4.2 kJ mol$^{-1}$ was calculated. The value for $\Delta_f H_o$ for HCN was taken

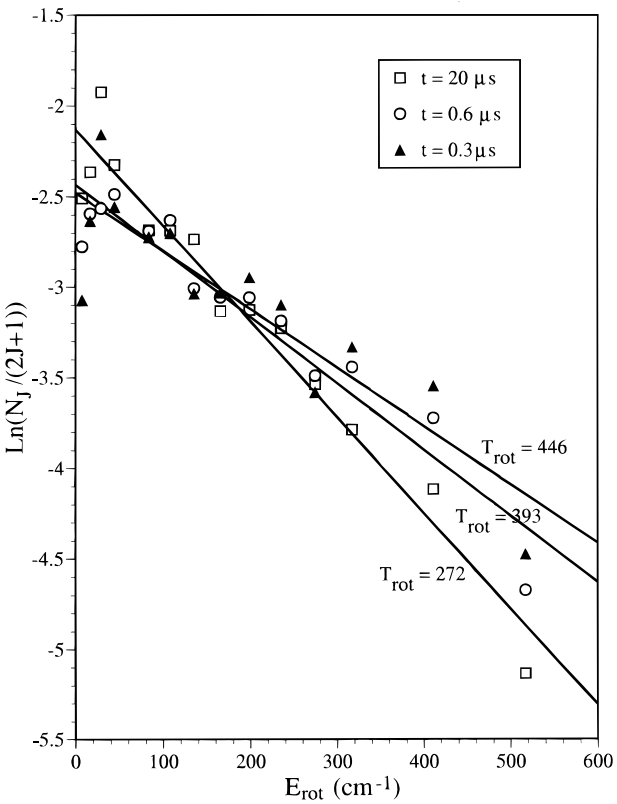


**Figure 6.** Boltzmann plot of the rotational state distributions shown in Figure 5.

**TABLE 2: Summary of the Energetics for the H + $(CN)_2$ → HCN/HNC + CN Reaction**

| reaction | $\Delta H°$ reaction (kJ mol$^{-1}$) | $\langle E_{avail}\rangle^a$ (kJ mol$^{-1}$) |
|---|---|---|
| H + $(CN)_2$b → HCN[c] + CN | 41.0 ± 10.2 | +54.5 |
| → HNC[d] + CN | 101 ± 14 | −6 |

[a] Calculated for $\langle E_T^H\rangle$= 92 kJ mol$^{-1}$ in eq 7. [b] $\Delta_f H°$ $(CN)_2$ = 307.2 ± 4 kJ mol$^{-1}$. Ref: Chase, M. W., Jr. *NIST-JANF Thermochemical Tables*; AIP; New York, 1998. [c] $\Delta_f H°$ HCN = 132.3 ± 4.2 kJ mol$^{-1}$. ref 35. [d] $\Delta_f H°$ HNC = 192.6 ± 8.2 kJ mol$^{-1}$. ref 36.

from the recent work of Berkowitz et al.,[35] and the value for $\Delta_f H°$ for HNC was taken from the theoretical calculation by Lee and Rendell.[36] The most probable energy available to the HNC + CN product channel, $\langle E_{avail}\rangle$ is given by

$$\langle E_{avail}\rangle = -\Delta H° + \langle E_T^H\rangle + RT + \langle E_\nu^{therm}\rangle \qquad (7)$$

where $\langle E_T^H\rangle$ is the average COM translational energy of the reacting H atoms, *RT* accounts for the reactant rotation energy, and $\langle E_\nu^{therm}\rangle$ accounts for the thermal excitation in the two degenerate low-frequency bending modes of $(CN)_2$ ($\langle E_\nu^{therm}\rangle$ = 1.1 kJ mol$^{-1}$). The relative collision energy between the H atom and $(CN)_2$ is essentially given by the initial translational energy of the H atoms because of the small mass of an H atom. For this mass combination, the contribution of reactant thermal motion to $\langle E_T^H\rangle$ can be ignored.[37] As summarized in the last column of Table 2, the HNC + CN product channel is calculated to be 6 kJ mol$^{-1}$ endothermic; however, the uncertainty in $\Delta H°$ and the broad distribution of the initial translational energy of the H atoms ($\bar{E}_T^H$) = 92, and fwhm = 38 kJ mol$^{-1}$) leads to a relatively large uncertainty in the actual threshold energy for the reaction. However, the fact that the products were observed to be produced almost entirely during the first 0.3 $\mu$s (Table 1) indicated that only the most energetic H atoms react to form HNC.

**TABLE 3: Determination of the HNC Vibrational State Distribution from the H + $(CN)_2$ → HNC + CN Reaction**

| boxcar delay | [HNC(000,$J$ = 9)] × 10$^{-9}$ (molecule cm$^{-3}$) | [HNC(000)]$_{tot}$ × 10$^{-10}$ (molecule cm$^{-3}$) | [HNC]$_{tot}$ × 10$^{-10}$ (molecule cm$^{-3}$) | [HNC(000)]$_{tot}$/[HNC]$_{tot}$ |
|---|---|---|---|---|
| 0.3 | 1.8 | 3.3 | 5.9 | 0.44 |
| 0.6 | 2.5 | 4.1 | 6.9 | 0.41 |
| 20.0 | 6.7 | 9.3 | 11. | 0.16 |

| | [HNC(010,$J$ = 9,e)] × 10$^{-8}$ (molecule cm$^{-3}$) | [HNC(010)]$_{tot}$ × 10$^{-10}$ (molecule cm$^{-3}$) |
|---|---|---|
| 0.3 | 6.7 | 2.6 |
| 0.6 | 8.2 | 2.8 |
| 20.0 | 6.2 | 1.8 |

[a] The initial vibrational level distribution of HNC was given by the distribution determined at the observation time of 0.3 $\mu$s. The uncertainty in the average of three measurements for [HNC($0v_2^l0$,$J$ = 9)] populations was about ±10%.

Only the transitions originating from HNC(000) and HNC($01^10$) were detected in the present work. The exact frequencies for other rovibrational transitions have been recorded in this laboratory,[23] but scans over the wavelength regions corresponding to several low $J$ transitions originating from the HNC($02^{0,2}0$) and HNC(001) vibrational levels were unsuccessful.

As noted previously, the [HNC($00^00$; $J$ = 9)] and [HNC($01^10$; $J$ = 9, 10] populations were used to normalize the population data obtained at various times and experimental conditions. Furthermore, the absorption technique results in an absolute determination of the population in each HNC rovibrational state. The initial vibrational population can be determined from the initial rotational state distribution for each vibrational level combined with the measurement of the population in a single rotational state for the various vibrational levels obtained under the same experimental conditions. The initial rotational state distributions for HNC($00^00$) and ($01^10$) were taken as that measured at an observation time of 0.3 $\mu$s., Figures 3 and 5, and were described by the $T_{rot}$ given in Table 1.

The results for the determination of [HNC($00^00$)]$_{tot}$ and [HNC($01^10$)]$_{tot}$ are summarized in Table 3. As is evident from the last column in Table 3, the fraction of the observed HNC produced in reaction 2b that was found in the HNC($01^10$) level was constant as the observation time increased from 0.3 to 0.6 $\mu$s, indicating that vibrational relaxation was negligible over this time interval. After 20 $\mu$s, the HNC vibrations had equilibrated to the temperature of the reaction chamber as indicated by the measured fraction of HNC that was in the HNC($01^10$) bending vibration. Even though the uncertainty in the determination of the population in an individual rotational state was estimated to be about ±10%, the excellent agreement with the expected thermal value provides confidence in the initial vibrational distribution measurement.

The total concentrations of HNC, [HNC]$_{tot}$, observed in the experiment at the various observation times are given in the second last column of Table 3. The [HNC]$_{tot}$ increased by a factor of 1.9 from the initial to the final observation time, whereas it only increased by a factor of 1.17 for a factor of 2 increase in reaction time. The same trend is evident in the data presented in Table 1 for each vibrational level. As noted earlier, reaction 3b produces HNC, and the observed increase in [HNC] at an observation time of 20 $\mu$s was due to this channel. The

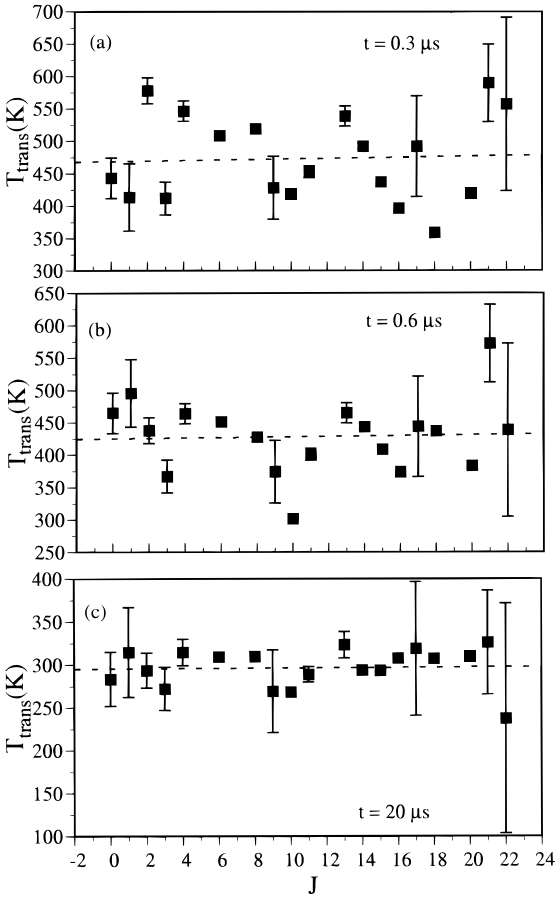


**Figure 7.** Summary of the determination of the laboratory translational temperatures at three observation times for the rotational states in the HNC($00^00$) vibrational manifold using the measured Doppler widths, according to Equation 8. The dashed line is a linear least-squares fit to the data, showing that there was no measurable correlation between $T_{trans}$ and J.

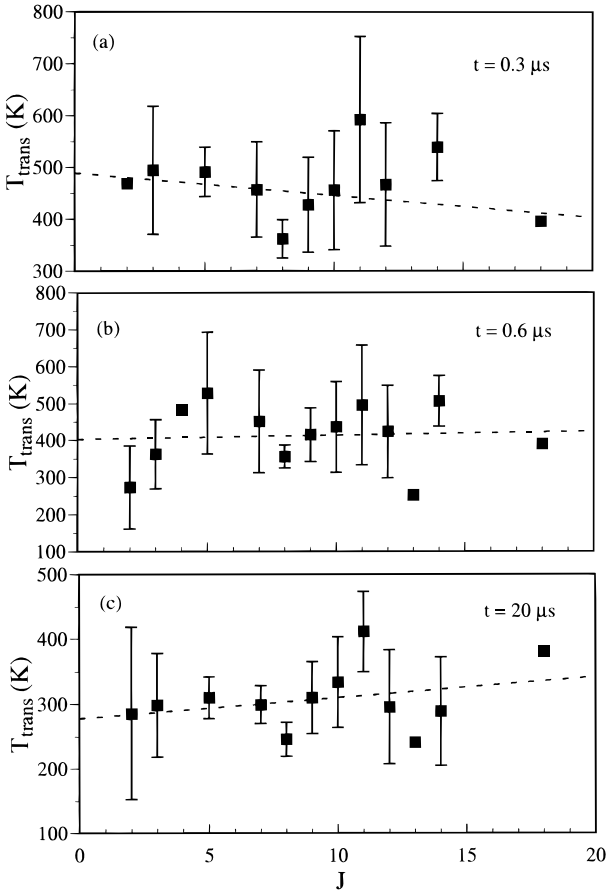


**Figure 8.** Similar to Figure 7 except for the HNC($01^10$) vibrational level.

**TABLE 4: Summary of the Determination of $\langle E_T^v \rangle$ for HNC(0 $v_2^1$ 0) Measured at Different Observation Times**

| vibrational level | observation time($\mu$s) | $T_{trans}$ (K) | $\langle E \rangle_T^v$(kJ mol$^{-1}$) |
|---|---|---|---|
| HNC($00^00$) | 0.3 | $473 \pm 68^b$ | $11 \pm 1.4$ |
| | 0.6 | $429 \pm 57$ | |
| | 20.0 | $297 \pm 23$ | |
| HNC($01^10$) | 0.3 | $449 \pm 89$ | $10 \pm 2$ |
| | 0.6 | $415 \pm 85$ | |
| | 20.0 | $308 \pm 49$ | |

[a] The $\bar{\nu}_D$'s were obtained by non-linear least squares fits to the A(v) profiles for each rotational state in the HNC($00^00$) and HNC($01^10$) vibrational levels, and $T_{trans}$ determined from eq 8 [b] The uncertainty is $\pm 1\sigma$ in the average $T_{trans}$ plotted in Figures 7 and 8.

fact that preliminary data[24] indicate that the branching fractions for the production of HNC in both reactions 2 and 3 are nearly equal implies that the final concentration of HNC, after reaction 3b has gone to completion, should be twice the initial concentration of HNC, as observed in Table 3.

**D. Translational Energy Release for H + $(CN)_2$ → HNC + CN.** Inspection of the absorbance profiles shown in Figures 1 and 2 shows that the HNC product from reaction 2b was formed with excess translational energy. It was argued in Section III A that the HNC speed distribution should be isotropic or nearly so. This, coupled with the fact that the absorbance profiles exhibited a Gaussian dependence on frequency, indicates that the laboratory speed distribution of HNC was described by a Maxwell−Boltzmann distribution.[38] The laboratory translational temperature, $T_{trans}$, is related to the fwhm of the absorbance profile, $\bar{\nu}_D$ (cm$^{-1}$), by

$$T_{trans} = \frac{M}{8R \ln 2} \frac{c^2}{\bar{\nu}_{ji}^2} \bar{\nu}_D^2 \qquad (8)$$

where $M$ (grams) is the mass of the probed molecule, and $R$ is the gas constant (ergs/degree). The average translational energy for the probed molecule in vibrational level $v$, $\langle E_T^v \rangle$, was taken as 1.5 $RT_{trans}$.

Plots of the measured $\bar{\nu}_D$'s for the rotational states of the HNC($00^00$) vibrational level at the three observation times are shown in Figure 7, and for the HNC($01^10$) level in Figure 8. The results are summarized in Table 4 as simple averages over all the rotational states of the $T_{trans}$ at each observation time. The dashed lines in Figures 7 and 8 are linear least-squares fits to the data. As is clear from these figures, the data were too scattered to exhibit any trends in the translational energy released as a function of the HNC rotational state. The error bars result from the repeated measurement of $\bar{\nu}_D$ for the same rotational state. At the final observation time of 20 $\mu$s, the measured $T_{trans}$ corresponded to the measured temperature of the reaction chamber, 293 K, within experimental scatter, indicating that the frequency scale was accurately calibrated by the Etalon fringe measurements. The $T_{trans}$ determined at the observation time of 0.3 $\mu$s was taken as a measure of the translational energy release in reaction 2b. The small change in $T_{trans}$ on going from an observation time of 0.3 to 0.6 $\mu$s indicated that translational relaxation was small under the conditions of the experiment, and the initial $T_{trans}$ for reaction 2b must be close to that observed

at 0.3 $\mu$s. A comparison of Tables 1 and 3 also reveals that $T_{rot}$ and $T_{trans}$ were equilibrated with each other, within experimental scatter.

For a discussion of the dynamics of reaction 2b, the desired quantity is the mean translational energy released in the COM collision frame, $\langle E_T \rangle$. The conversion from the laboratory frame to the COM frame requires knowledge of the differential cross section, which is unknown. However, some idea of the COM translational energy release can be obtained by taking advantage of the near isotropic H atom distribution to relate the laboratory and COM speed distributions of HNC. The laboratory velocity of an HNC product molecule, $\boldsymbol{v}_{\mathbf{HNC}}$, produced in a single reactive collision is the vector sum of the COM velocity $\boldsymbol{v}_{\mathbf{COM}}$ and the COM velocity of HNC, $\boldsymbol{u}_{\mathbf{HNC}}$, i.e., $\boldsymbol{v}_{\mathbf{HNC}} = \boldsymbol{v}_{\mathbf{COM}} + \boldsymbol{u}_{\mathbf{HNC}}$. The differential cross section determines the final angle between $\boldsymbol{v}_{\mathbf{COM}}$ and $\boldsymbol{u}_{\mathbf{HNC}}$. Even though the most probable initial[25] H atom speed is high, $1.4 \times 10^6$ cm s$^{-1}$, its mass is only 1.9% of the mass of $(CN)_2$, and $\boldsymbol{v}_{\mathbf{COM}}$ is only slightly deviated from the initial $(CN)_2$ velocity; thus, the approximation $\boldsymbol{v}_{\mathbf{COM}} \approx \boldsymbol{v}_{\mathbf{(CN)2}}$ is reasonable. Furthermore, $\boldsymbol{v}_{\mathbf{(CN)2}}$ has an isotropic Maxwell−Boltzmann distribution. The velocity of HNC in the COM system can be approximated by $\boldsymbol{u}_{\mathbf{HNC}} \approx \boldsymbol{v}_{\mathbf{HNC}} - \boldsymbol{v}_{\mathbf{(CN)2}}$, where both $\boldsymbol{v}_{\mathbf{HNC}}$ and $\boldsymbol{v}_{\mathbf{(CN)2}}$ are given by isotropic Maxwell−Boltzmann distributions. To determine the COM translational energy release in reaction 2b, the squared distribution of $u_{HNC}$ is needed. This is obtained from two Maxwell−Boltzmann distributions related by $u_{HNC}2 = v_{HNC}2 + v_{(CN)2}{}^2 - 2\, v_{HNC}\, v_{(CN)2}\cos\theta$, where $\theta$ is the angle between $\boldsymbol{v}_{\mathbf{HNC}}$ and $\boldsymbol{v}_{\mathbf{(CN)2}}$. This situation is identical to that described by Dagdigian et al.[39] These workers determined the relative speed-squared distributions for collisions of gases at two temperatures and found that the most probable speed squared was given by the sum of the most probable speeds squared for each gas, i.e., $\bar{u}^2_{HNC} = \bar{v}^2_{HNC} + \bar{v}^2_{(CN)2}$, where the bar indicates the most probable speed and $\bar{v}^2_X = \sqrt{2kT/m_x}$, for molecule X. The conservation of linear momentum in the COM frame allows the most probable relative translational energy in the COM frame, $\langle E_T \rangle$, to be given by $\langle E_T \rangle = 1/2\ m_{HNC}/m_{CN}(m_{HNC} + m_{CN})\ \bar{u}^2_{HNC}$.

The last column in Table 4 gives the measured $\langle E_T \rangle$ as determined after 0.3 $\mu$s. Even though the HNC($01^10$) vibrational level is 5.55 kJ higher in energy than the ground state the translational energy release is similar within experimental error for each vibrational level.

**E. Absolute Reaction Cross Section for H + $(CN)_2$ → HNC + CN.** As summarized in Table 3, the measurements reported in this work provide a determination of the absolute concentration of the HNC product and can be used to determine an estimate of the reaction cross section, $\sigma_R$, for reaction 2b provided some estimate of the concentration and speed of the reacting H atoms can be made. This was done by making the following approximations. Above the reaction threshold, $\sigma_R$ was assumed to be independent of the H atom collision energy, and the reaction threshold was taken to occur for H atoms with translational energy greater than the reaction endothermicity, i.e., 98 kJ mol$^{-1}$ (Table 2). The concentration of H atoms with translational energy greater than the reaction threshold, $[H]_R$, corresponds to 0.23 of the total number of atoms created in the photolysis of $CH_3SH$. The reaction rate constant, $k_{2b}$, can be estimated from $k_{2b} = \sigma_R \langle v_H \rangle$, where $\langle v_H \rangle$ is the average speed of the H atoms that can react, and was calculated from $\langle v_H \rangle = \int_{Eth}^{\infty} vP(v)dv = 1.5 \times 10^6$ cm s$^{-1}$, where $P(v)$ is the normalized Gaussian speed distribution of the H atoms.

Under near single collision conditions, such as the case here, the H atoms lost by reaction are equal to the total production of products, $[HNC]_{tot}$. The kinetic rate equation describing the loss of H atoms can be rearranged to give $\sigma_R$ as

$$\sigma_R = \frac{[HNC]_{tot}}{\langle v_H \rangle [H]_R\, [(CN)_2] \Delta t} \tag{9}$$

where $\Delta t$ is the observation time at which the $[HNC]_{tot}$ was measured. Equation 9 implies a linear relationship between the observation time and the accumulation of product; i.e., the measurement of the number density is equivalent to the reactive flux. Previously, this equivalence was demonstrated for reaction 2 using the same experimental apparatus and conditions, except monitoring the CN($v = 0$; $J$) product.[20] For reaction 2b, the $[HNC]_{tot}$ was found to increase by 17% as the observation time increased by a factor of 2; however, this is not due to a violation of the equivalence between reactive flux and number density but rather to the relaxation of the H atom translational energy distribution. Only a small shift in the H atom energy distribution to lower energies is needed to quench reaction 2b.

The cross section for absorption of $CH_3SH$ and the quantum yield for H atom production at 248 nm have been measured to be $3.0 \times 10^{-19}$ cm$^2$ molecule$^{-1}$and 1, respectively.[26] The photolysis laser energy was measured directly in front of the entrance window of the reaction chamber, but the actual laser energy that traversed the apparatus was not measured directly. Estimates of the loses on the entrance window and UV−IR dichroic were made to determine the actual photolysis laser energy irradiating the photolysis zone. Using the measurement of the $[HNC]_{tot}$ at an observation time of 0.3 $\mu$s provided in Table 3 and eq 9, the $\sigma_R$ for reaction 2b was calculated to be $2.0 \times 10^{-18}$ cm$^2$ for an $\langle E_T^H \rangle$ of 113 kJ mol$^{-1}$. The uncertainty in determining $\sigma_R$ was estimated to be about a factor of 2 primarily because of the uncertainty in determining the $[H]_R$ atoms.

## IV. Discussion

The measurements of the present work provide a comprehensive look at the complete energy disposition into the HNC product from reaction 2b by detailing how the reaction energy was shared among all the degrees of freedom: translation, rotation, and vibration. Unfortunately, the energetics were not well-defined because of the initial broad H atom translational energy distribution. Assuming $\langle E_T^H \rangle$ to be 113 kJ mol$^{-1}$(see Section III D), $\langle E_{avail} \rangle$ can be calculated to be 18.5 kJ mol$^{-1}$. Another estimate for $\langle E_{avail} \rangle$ can be made using the measurements of the HNC product state distribution and the COM translational energy release. The most energetic rotational state observed for each vibrational level can be identified from Figure 3 for HNC($00^00$) and Figure 5 for HNC($01^10$) to be $J = 22$ and $J = 18$, respectively. Using the $\langle E_T^v \rangle$ for each vibrational level (Table 4), the maximum energies available to the HNC($00^00$) and ($01^10$) product states are 20.1 and 21.7 kJ mol$^{-1}$, respectively. Of course, this is a crude estimate of $\langle E_{avail} \rangle$ insofar as more energetic states were not detected because of signal-to-noise limitations, and the CN($v = 0$, J) coproduct must be assumed to be in $J = 0$. Nevertheless, the estimates of $\langle E_{avail} \rangle$ using the two methods are in reasonable agreement. Because the product state distribution estimate relied on a value of $\langle E_T^v \rangle$ that is clearly an overestimate of the translational energy of the most thermodynamically allowed product state, a value of $\langle E_{avail} \rangle = 19$ kJ mol$^{-1}$ was taken as a reasonable estimate. With this value of $\langle E_{avail} \rangle$, HNC bending vibrations up to $\nu_2 = 3$ could have been excited.

**TABLE 5: Summary of the Estimates for the Complete Energy Disposition into Vibration, Rotation, and Translation for the H + $(CN)_2$ → HNC + CN Reaction**

| | vibrational level | |
|---|---|---|
| | (000) | ($01^10$) |
| $\langle E_{avail}\rangle - E_v$ (kJ mol$^{-1}$) | 19 | 13.4 |
| $f_T^v$ | 0.57 | 0.75 |
| $f_R^{HNC(v)}$ | 0.22 | 0.27 |
| $f_R^{v,CN(0)}$ | 0.20 | ~0 |

[a] The $\langle E_{Avail}\rangle$ was estimated to be 19 KJ mol$^{-1}$. Only HNC($0v_2^l$ 0) for $v_2 = 0^0$ and $1^1$ were detected experimentally.

The rotational energy content of the CN fragment, produced along with HNC in reaction 2b is unknown; however, the combined average rotational energy for CN produced in both reactions 2a and 2b has been measured[20] to be 7.4 kJ mol$^{-1}$. Reaction 2a is 60 kJ mol$^{-1}$ more exothermic than reaction 2b and accounts for about 90% of the total reaction rate. The rotational excitation of CN produced in reaction 2b should not be more than that of the HNC($00^00$) and ($01^10$), products, 4.2 and 3.7 kJ mol$^{-1}$, respectively. The average rotational energy content of the CN coproduct can be estimated from the conservation of energy equation:

$$\langle E_{avail}\rangle = \langle E_T^v\rangle + \langle E_R^{HNC(v)}\rangle + E_v^{HNC} + \langle E_R^{HNC(v)}\rangle \quad (10)$$

where $\langle E_R^{v,X}\rangle = RT_{rot}$ is the average rotational energy content of species X in vibrational level $v$, and $E_v^{HNC}$ is the vibrational energy of level $v$.

The results are summarized in Table 5 expressed as the fraction of the available energy in vibrational level v that appeared as COM translational energy and rotational energy of HNC or CN. The $\langle E_R^{HNC(v)}\rangle$ was determined from the $T_{rot}$ measured at the earliest observation time listed in Table 1, and $\langle E_T^v\rangle$ is given in Table 4. It has been argued previously[20] that on purely kinematic grounds, the $\langle E_R^{HNC(v)}\rangle$ should be similar to $\langle E_R^{v,CN(0)}\rangle$ for reaction 2. This is approximately true for the CN produced along with the HNC($00^00$) level, but not so for CN produced along with HNC($01^10$). The difference is attributed to the large uncertainty in the estimate of $\langle E_{avail}\rangle$ and experimental scatter in the determination of $\langle E_T^v\rangle$. It is more likely that $\langle E_R^{v,CN(0)}\rangle \approx \langle E_R^{HNC(v)}\rangle$ for all HNC vibrations.

An interesting aspect of the results in Table 5 is the increased partitioning of the available energy into the translational energy of the separating fragments on going from $v_2 = 0$ to $v_2 = 1$. As noted above, there is considerable uncertainty in the determination of the translational energy (Table 4); however, this may be a real trend as even $f_R^{HNC(v)}$ is larger for $v_2 = 1$ than for $v_2 = 0$.

Using the estimates for the energy partitioning summarized in Table 5 and the observed vibrational state distribution, the global energy disposition for each degree of freedom was calculated, expressed as a fraction of the $\langle E_{avail}\rangle$ that appears in a particular degree of freedom summed over the vibrational population. The results are summarized in Table 6 along with similar results for related triatomic reaction systems: H + $F_2$ → HF + F[40] and H + $Cl_2$ → HCl + Cl.[41]

Both the mass and electron affinity[42] of the CN radical lie between those of the F and Cl atom; however, the global dynamical features appear to be quite similar to the H + $Cl_2$ reaction system (Table 6). It appears that the global features of energy partitioning for a polyatomic reaction system can be rationalized from the observations of triatomic systems of similar mass combinations,[1] i.e., **L + H−H** reaction systems. One difference between the polyatomic and the triatomic case is the linear or nearly linear nature of the reactive configurations in the triatomic situation. The PESs for both H + HCN[43] and H + ClCN[18] were found to be highly repulsive for linear H−N configurations, and it is presumed that reaction 2 proceeds through bent configurations.

**TABLE 6: Summary of the Global Fraction of $\langle E_{Avail}\rangle$ that Appeared as Product Translation, Rotation, and Vibration for Reaction 2bl**

| reaction | $\langle f_T\rangle$ | $\langle f_R\rangle$ | $\langle f_V\rangle$ |
|---|---|---|---|
| H +$(CN)_2$→HNC + CN ($E_{avail} \approx 19$ kJ mol$^{-1}$) | 0.56 | 0.32 | 0.13 |
| H + $F_2$→HF + F[b] ($E_{avail}$=427 kJ mol$^{-1}$) | 0.39 | 0.03 | 0.58 |
| H + $Cl_2$→HCl + Cl[c] ($E_{avail}$=203 kJ mol$^{-1}$) | 0.54 | 0.09 | 0.37 |

[a] For comparison, the energy disposition for the related H + $X_2$ reactions are included, where X is F or C. [b] Ref 40. [c] Ref 41.

The PES describing the HNCCN system has not been explored in as much detail as that available for the HClCN system; however, Yang et al.[44] have described several stationary points on the HNCCN surface at the BAC-MP4 level of theory. These workers found that an NC(H)CN adduct was bound by about 130 kJ mol$^{-1}$ with respect to the H + $(CN)_2$ asymptote. It is clear from the average energy disposition, Table 6, that the product state distribution is highly nonstatistical so that the formation of a long-lived complex, in which the energy in the internal degrees of freedom are completely randomized, appears unlikely. The presence of a deep potential minimum on the HNCCN surface could facilitate the occurrence of secondary encounters, however.

One major difference between the polyatomic and triatomic reaction systems (Table 6) is the large fraction of the internal energy that appears as product rotation compared to vibration in the polyatomic case. To excite rotational motion in a molecule, a torque must be applied about its COM. For the triatomic systems, this is difficult because the reaction exothermicity is released repulsively between the diatomic fragment in linear or near linear configurations. Furthermore, the COM of the diatomic product lies close to the halogen atom, making rotational excitation again unfavorable. However, for the H + $(CN)_2$ system, near-linear configurations are highly repulsive, and the reaction must proceed through bent configurations. Under such circumstances, the COM of the new HNC product molecule is not collinear with the direction of the repulsive energy release between the two C atoms, and a large torque can be applied to the departing fragments, HNC and CN. Also, the anisotropy of the PES between a diatomic and linear triatomic molecule should be greater than that between an atom and a diatomic hydride molecule. Both of these factors favor rotational excitation in the polyatomic product case.

Another difference between reaction 2b and the H + halogen reactions is the small amount of energy available to the products for the former reaction (Table 6). For reaction 2b, this small value of $\langle E_{avail}\rangle$ results in the rather small value for the relative velocity between the diatom and triatom fragments so that there is a high likely hood that secondary encounters can occur. In fact, for an HNC($0\ v_2^1\ 0$) molecule, with $J$ at the peak of the rotational state distribution, the CN and HNC fragments only separate 0.3 Å before HNC completes one rotational period. Such trajectories might be responsible for the conversion of initial bending vibrational motion into product rotation.

The reaction of energetic H atoms with XCN compounds, where X is Br, Cl, or CN, has been recently studied[20] by

monitoring the CN(0; *J*) product. Both the rotational state distribution of CN and the COM translational energy distribution were determined in these experiments. For reaction 2, the HCN channel accounts for nearly 90% of the products[24] and dominates the HNC pathway; hence, the observed CN(0; *J*) distribution can be attributed to the HCN channel. This channel is 60 kJ $mol^{-1}$ more energetic than the HNC channel; however, the $\langle f_T \rangle$ values are remarkably similar. The origins of these $\langle f_T \rangle$ values should be quite different in the two cases. He, Tokue, and Macdonald argued that the large $\langle f_T \rangle$ for the HCN channel arose from the tendency for **L** + **H**−**H** reaction systems to channel reactant translational energy greater than the barrier height into product translational energy. This cannot be the case for reaction 2b because the H atoms that react must just have enough energy to do so. It may be that the observed HNC molecules must have sufficient translational energy to separate from the CN radical otherwise the H atom could be transferred back to the departing CN radical and form the more exothermic reaction product, HCN.

## V. Summary

The reaction dynamics of translationally energetic H atoms with $(CN)_2$ was investigated by determining the complete initial rovibrational state distribution of HNC(0 $v_2^1$ 0), $v_2^1 = 0^0$, $1^1$, the minor product channel for reaction 2. The initial rotational state distributions for each vibrational level, $v_2^1 = 0^0$, $1^1$, were found to be Boltzmann, with $T_{rot} = 500 \pm 30$ and $440 \pm 80$ K, respectively. The initial vibrational distribution was found to have 44% of the observed HNC product in the first excited bending vibration, Table 3. As well, the initial COM translational energy released in each vibrational level was determined from the line width of the HNC absorption features, and the $T_{trans}$ for each vibrational level was found to be $470 \pm 70$ and $450 \pm 90$ K, for $v_2^1 = 0$, 1, respectively, Table 4. Within the scatter of the measurements the initial translational and rotational temperatures were equilibrated. Several methods were used to determine $\langle E_{avail} \rangle$, and an estimate of 19 kJ $mol^{-1}$ was used to calculate the fraction of the available energy in a given vibrational level that appeared as translation and rotation of both HNC and CN. The results are summarized in Table 5. The global disposition of the reaction energy is summarized in Table 6. As anticipated from studies of triatomic systems, the kinematics of **L** + **H**−**H** systems plays an important role in the global dynamics for polyatomic systems, and a large fraction of the energy released in the reaction appears as product translational motion.

Reaction 2b must occur through bent configurations so that bending and rotational motions are excited as the reaction energy is released between the departing C−C atoms. It was suggested that secondary encounters between the separating HNC and CN fragments could play an important role in determining the observed internal state distribution of HNC especially because of the small value for $\langle E_{avail} \rangle$. Clearly, detailed dynamics calculations on a PES that accounts for the interaction of the H atom attacking the N atoms in $(CN)_2$ will be needed to fully understand the dynamics in this five atom system.

**Acknowledgment.** The author wishes to thank Prof. I. Tokue and Dr. G. He for their work in carrying out preliminary experiments on the H + $(CN)_2$ system. This work was supported by the U.S. Department of Energy, Office of Basic Energy Sciences, Division of Chemical Sciences, under Contract W-31-109-ENG-38.

## References and Notes

(1) Polanyi, J. C. *Science* **1987**, *236*, 680.
(2) Holmes, B. E.; Setser, D. W. In *Physical Chemistry of Fast Reactions*; Smith, I. W. M., Ed.; Plenum Press: New York, 1980; Vol. 2, Chapter 2.
(3) Clary, D. C. *Science* **1998,** *279*, 1879.
(4) McDonald, J. D. *Annu. Rev. Phys. Chem.* **1979**, *30*, 29.
(5) Sugawara, K.; Fumiyuki, I.; Nakanaga, T.; Matsumura, C. *J. Chem. Phys.* **1990**, *92*, 5328.
(6) Arunan, E.; Setser, D. W. *J. Phys. Chem.* **1991**, *95*, 4190.
(7) Frost, M. J.; Sharkey, P.; Smith, I. W. M. *Faraday Discuss. Chem. Soc*. **1991**, *91*, 305.
(8) Suzuki, T.; Hirota, E. *J. Chem. Phys*. **1993**, *98*, 2387.
(9) Arunan, E.; Manke, G., II; Sester, D. W. *Chem. Phys. Lett*. **1993**, *207*, 81.
(10) Nizamov, B.; Setser, D. W. *J. Phys. Chem*. **1996**, *100*, 4853.
(11) Phillips, L. F.; Smith, I. W. M.; Tuckett, R. P.; Whitham, C. J. *Chem. Phys. Lett.* **1991**, *183*, 254.
(12) Sauder, D. G.; Patel-Misra, D.; Dagdigian, P. J. *J. Chem. Phys*. **1991**, *95*, 1696.
(13) Macdonald, R. G.; Liu, K.; Sonnenfroh, D. M.; Liu, D.-J. *Can. J. Chem*. **1994**, *72*, 660.
(14) Schatz, G. C. *J. Phys. Chem*. **1996**, *100*, 12 839.
(15) Clary, D. C. *J. Phys. Chem*. **1994**, *98*, 10 678.
(16) Bowmann, J. M.; Schatz, D. C. *Annu. Rev. Phys. Chem*. **1996**, *46*, 169.
(17) Casavecchia, P.; Balucani, N.; Volpi, G. G. *Annu. Rev. Phys. Chem*. **1999**, *50*, 347.
(18) Harding, L. B. *J. Phys. Chem*. **1996**, *100*, 10 123.
(19) Nizamov, B.; Setser, D. W.; Wang, H.; Peslherbe, G. H.; Hase, W. L. *J. Chem. Phys*. **1996**, *105*, 9897.
(20) He, G.; Tokue, I.; Macdonald, R. G. *J. Chem. Phys*. **2000**, *112*, 6689.
(21) Bethardy, G. A.; Northrup, F. J.; He, G.; Tokue, I.; Macdonald, R. G. *J. Chem. Phys.* **1998**, *109*, 4224.
(22) Burkholder, J. B.; Sinha, A.; Hammer, P. D.; Howard, C. *J. Mol. Spec*. **1987**, *126*, 72.
(23) Northrup, F. J.; Bethardy, G. A.; Macdonald, R. G. *J. Mol. Spec*. **1997**, *186*, 349.
(24) Decker, B. K.; Macdonald, R. G., in preparation.
(25) Rogers, L. J.; Ashfold, M. N. R.; Matsumi, Y.; Kawasaki, M.; Whitaker, B. J. *J. Chem. Soc., Faraday Trans*. **1996**, *92*, 5181.
(26) Barone, S. B.; Turnipseed, A. A.; Gierczak, T.; Ravishankara, A. R. *J. Phys. Chem*. **1994,** *98*, 11 969.
(27) Jensen, E.; Keller, J. S.; Waschewsky, G. C. G.; Stevens, J. E.; Graham, R. L.; Freed, K. F.; Butler, L. J. *J. Chem. Phys*. **1993**, *98*, 2882.
(28) Park, J.; Shafer, N.; Bersohn, R. *J. Chem. Phys*. **1989,** *91*, 7861.
(29) Kroto, H. W. *Molecular Rotational Spectra*; Dover: New York 1992; p 69.
(30) He, G.; Macdonald, R. G. *Chem. Phys. Lett*. **1999**, *301*, 175.
(31) Smith, M. A. H.; Rinsland, C. P.; Fridovich, B. *Molecular Spectroscoy: Modern Research*; Rao, K. N. Ed.; Academic Press: Orlando, 1985.
(32) Nezn, M.; Ammano, T.; Kawaguchi, K. *J. Mol. Spect*. **1998,** *192*, 41.
(33) Press, W. H.; Flannery, B. P.; Teukolsky, S. A.; Vetterling, W. T. *Numerical Recipes: The Art of Scientific Computing*; Cambridge University: Cambridge, 1988; Chapter 14.
(34) North, S. W.; Hall, G. E. *J. Chem. Phys*. **1997**, *106*, 60.
(35) Berkowitz, J.; Ellison, G. B.; Gutman, D. *J. Phys. Chem*. **1994**, *98*, 2744.
(36) Lee, T. J.; Rendell, A. P. *Chem. Phys. Lett*. **1991**, *177*, 491.
(37) Zande, W. J.; Zhang, R.; Zare, R. N.; McKendrick, K. G.; Valentini, J. J. *J. Phys. Chem*. **1991**, *95*, 8205.
(38) Gordon, R. J.; Hall, G. E. *Advances in Chemical Physics*; Prigogine, I., Rice, S. A., Eds.; John Wiley & Sons: New York, 1996; Chapter 1.
(39) Dagdigian, P. J.; Cruse, H. W.; Zare, R. N. *J. Chem. Phys*. **1975,** *62*, 1824.
(40) Polanyi, J. C.; Sloan, J. J. *J. Chem. Phys*. **1972**, *57*, 4988.
(41) Anlauf, K. G.; Horne, D. S.; Macdonald, R. G.; Polanyi, J. C.; Woodall, K. B. *J. Chem. Phys*. **1972**, *57*, 1561.
(42) Tyler, J. K.; Sheridan, J. *Trans. Faraday Soc*. **1963**, *59*, 2661.
(43) ter Horst, M. A.; Schatz, G. C.; Harding, L. B. *J. Chem. Phys*. **1996**, *105*, 558.
(44) Yang, D. L.; Yu, T.; Lin, M. C.; Melius, C. F. *J. Chem. Phys*. **1992**, *97*, 222.